

Slow-Neutron Scattering and Collective Motions in Liquid Lead*

P. D. RANDOLPH†

Phillips Petroleum Company, Idaho Falls, Idaho

AND

K. S. SINGWI

Argonne National Laboratory, Argonne, Illinois

(Received 22 June 1966)

Using the Materials-Testing-Reactor phased-chopper velocity selector, measurements have been made of the scattering law $S(\kappa, \hbar\omega)$ for liquid lead at 352°C for energy transfers $\hbar\omega$ in the range 0–20 meV and for momentum transfer $\hbar\kappa$ in the range 1–4 Å⁻¹. The scattering law exhibits a strong momentum-dependent structure at small energy transfer (corresponding to the diffraction maxima). Although for large values of the energy transfer this pronounced structure has disappeared, the $S(\kappa, \hbar\omega)$ curves still show two very broad maxima. The “one-phonon” partial differential scattering cross section is extracted from the data after subtracting multiphonon and multiple-scattering contributions, and the results are compared with those calculated on the basis of a model proposed by one of us (K.S.S.). This comparison shows that the model not only has the correct qualitative features but also gives a semi-quantitative agreement. From the analysis of the data, we conclude that there exist “collective excitations” in liquid lead. Also, for times of the order of 10⁻¹² sec, there exist at least the first two somewhat diffuse Brillouin zones in the liquid.

I. INTRODUCTION

DURING recent years considerable progress has been made in our understanding of the dynamical behavior of atoms in a liquid through slow-neutron scattering experiments. These experiments measure the dynamical structure factor $S(\kappa, \omega)$, which, in principle, furnishes complete information about the space-time correlations of atoms. In actual practice, the knowledge of $S(\kappa, \omega)$ is restricted by experimental limitations to a finite range of the values of momentum transfer $\hbar\kappa$ and energy transfer $\hbar\omega$. Nevertheless, it has been possible to extract a good deal of relevant physical information about the dynamics of the system. For example, from the results of an earlier experiment¹ on liquid sodium it was deduced that the mean-square displacement² of an atom as a function of time is not at all simple-diffusive in character, but is more solid-like, at least for times of the order of 10⁻¹² sec. A similar conclusion for liquid lead has also been reached by several workers.^{3–5} The liquid-sodium experiment also showed the presence of typical coherence effects which could be understood⁶ at least qualitatively on the basis

of a quasi-crystalline model proposed by one of us.^{7,8} We shall henceforth call this the QC model.

In this paper we report a detailed and more careful experimental study of $S(\kappa, \hbar\omega)$ as a function of κ in the range $\kappa=1$ to 4 Å⁻¹ for $\hbar\omega$ values in the range 0 to 20 meV, for liquid lead at 352°C. This experiment was undertaken with two main purposes in mind: (a) Since lead, besides being an interesting simple metal with a low melting point, is a completely coherent scatterer, the interference effects in the inelastic scattering in the liquid will be most pronounced. It was desirable therefore to see if we could understand these coherent effects in terms of collective excitations in a classical liquid. (b) We wanted to make a more detailed and, if possible, a quantitative comparison with the predictions of the QC model.^{7,8} Our results can be summarized as follows: First, in spite of the crudeness of the model, it is in surprisingly good agreement with our data. Second, a linear average dispersion law for “quasiphonons” with a velocity of sound approximately equal to 1.8×10⁵ cm/sec seems to account reasonably well for our experimental observations. And last, there are indications of the presence of at least the first two Brillouin zones, though they are diffuse, in liquid lead near its melting point.

In Sec. II we give details of some of the modifications and changes in the experimental apparatus which have not been previously published. Experimental details are given in Sec. III, and the data are presented in Sec. IV. Pertinent formulas based on the model are outlined in Sec. V, and a comparison of the experimental results with the calculations is made in Sec. VI. Section VII summarizes our conclusions.

⁶ K. S. Singwi and G. Feldman, in *Inelastic Scattering of Neutrons in Solids and Liquids* (International Atomic Energy Agency, Vienna, 1965), Vol. II, p. 85.

⁷ K. S. Singwi, Phys. Rev. **136**, A969 (1964).

⁸ K. S. Singwi, Physica **31**, 1257 (1965).

* Based on work performed under the auspices of the U. S. Atomic Energy Commission.

† Now with Idaho Nuclear Corporation, Idaho Falls, Idaho.

¹ P. D. Randolph, Phys. Rev. **134**, A1238 (1964).

² A much more sensitive criterion for a departure from the simple-diffusive kind of motion is to look for the frequency dependence of the Fourier transform $f(\omega)$ of the velocity-autocorrelation function. The latter is a Lorentz function for a simple diffusive motion. The actual $f(\omega)$ has a maximum value for a certain ω and then tends to zero.

³ S. J. Cocking and Z. Guner, in *Inelastic Scattering of Neutrons in Solids and Liquids* (International Atomic Energy Agency, Vienna, 1963), Vol. I, p. 237.

⁴ S. J. Cocking and P. A. Egelstaff, Phys. Letters **16**, 130 (1965).

⁵ H. Palevsky, in *Inelastic Scattering of Neutrons in Solids and Liquids*, (International Atomic Energy Agency, Vienna, 1961), p. 265.

II. APPARATUS CHANGES

A. Modifications of the Velocity Selector

The basic complete report on this apparatus and its construction has been given earlier by Brugger and Evans.⁹ Within the last few years, however, several changes have been made to improve its performance. The major modifications consist of new rotating collimators and higher speed operation. The two 11.4-cm-diam, phenolic-lined steel rotating collimators have been replaced by 30.5-cm diam nylon collimators. These have greatly reduced the background at short times of flight. Figure 1 shows a comparison of the steel and the nylon collimators at a speed of 6000 rpm. The reduction in background at short times of flight is by a factor of approximately 20. These collimators are designed for 6000 rpm operation when the choppers are at 12 000 rpm and therefore pass two bursts per revolution. The nylon collimator has a single symmetric slot with curved sides in it. The curvature is such that the slot is wider at each end than in the center. The beam size remains at 10.2-cm high and 3.3-cm wide.

The resolution of the velocity selector has been improved in the last few years by increasing the chopper speed while maintaining the same chopper slot width. The higher speed was accomplished by the use of different drive motors,¹⁰ and by a change in the design of the aluminum windows in the rotor insert. In the new design, the ribs of the windows are perpendicular to the rotation axis rather than parallel in order to take the increased radial stress at higher speeds. An advantage of this arrangement is that no epoxy is needed to fasten the windows to the chopping foils. The insert package is merely assembled in its clamp, then put into the chopper rotor. With such windows, the choppers have been spun up to 15 000 rpm, though normal operation is at 12 000 or 7500 rpm, depending on the energy range desired.

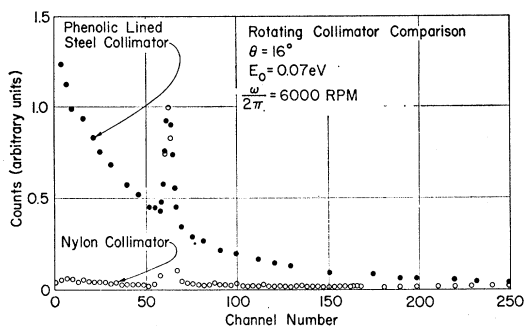


Fig. 1. Comparison of the nylon rotating collimators (12-in diam) with the phenolic-lined steel collimators (4½-in. diam).

⁹ R. M. Brugger and J. E. Evans, Nucl. Instr. Methods **12**, 75 (1961).

¹⁰ Hysteresis synchronous motors, ¼ hp, 400 cps, obtained from Electric Indicator Company, Inc., Stamford, Connecticut.

B. New Beam Hole

The velocity selector has been moved from the HG-6 beam hole to the high-flux HT-1 North through-hole of the Materials Testing Reactor. A report on flux measurements and the reflector geometry used in HT-1 has been given.¹¹ Since no report has been published on the changes in the velocity selector performance due to the move, it is included here.

Figure 2 shows a plan view of the velocity selector at the new beam hole HT-1 North. The main difference in the rotor arrangements is that the first collimator (A)

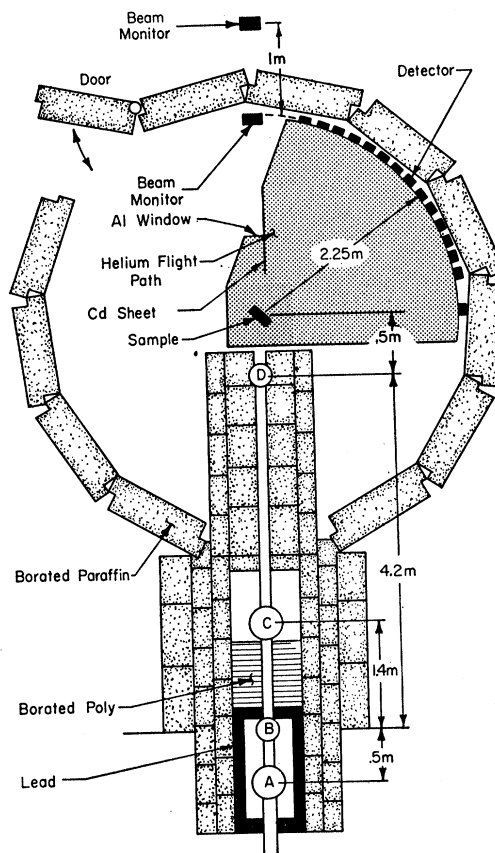


Fig. 2. Plan view of the velocity selector at the HT-1 through-hole showing the chopper arrangements, pertinent distances, and the helium-filled flight path.

has been placed ahead of the first chopper (B). A computer calculation of the transmission of the complete four-rotor system showed that for 12 000 rpm operation at a rotor phase setting corresponding to 0.04 eV, this arrangement would transmit fewer fast neutrons than if the chopper were placed before the collimator. Provisions have been made, however, to change this arrangement should it be desired. Also, with the collimator right at the reactor face inside the cubicle, its shielding can be made more effective. The

¹¹ R. M. Brugger, Nucl. Instr. Methods **32**, 303 (1965).

distance between the various rotors has been increased, and these distances are shown in Fig. 2. The scattered-neutron flight path has been increased from 2.00 to 2.25 m to help improve energy resolution. The helium flight path shown in the figure was installed for this particular experiment and will be discussed later.

The counting rate was expected to increase by a factor of 15 when moving to the new hole. However, because of different chopper arrangements and distances, the measured increase was a factor of 12.7 (at 0.04 eV). To increase the intensity further, the slot width of the first chopper (B) was increased from 0.081 cm to 0.162 cm, leaving the second chopper (D) unchanged. This resulted in an additional increase of counting rate by a factor of 2.7 at 0.04 eV. The broadening in energy resolution due to this change, however, was only a factor of 1.14, as measured by the time-of-flight distribution at the beam monitor.

III. EXPERIMENTAL DETAILS

A. Details of the Lead Experiment, the Sample, and Resolution

For this experiment the momentum transfers of primary interest are in the region $1\text{--}4 \text{ \AA}^{-1}$ around the first diffraction maximum at 2.2 \AA^{-1} . To confine the region of the measurement to these values, the BF_3 detector banks were located every 5° at 15 angles between 15° and 90° . The scattered-neutron flight path was 2.25 m from the sample to each detector. Each bank consisted of three 1-in. diam 18-in. long counters, which subtend a scattering angle of 1.96° at the sample. This gives a resolution in this range of κ of $\Delta\kappa \approx \pm 0.05 \text{ \AA}^{-1}$ for most angles and energy transfers.

The sample was in the form of a rectangular slab having a window 11.43 cm high by 7.62 wide of nominal thickness 0.127 cm. It is constructed of two steel frames sandwiching the 0.127-cm steel spacer and the windows. The windows were 0.0025-cm vanadium sheet. Vanadium was used for the window material because it is a completely incoherent scatterer and thus cannot introduce any extraneous coherent effects. Also, it has a smaller thermal expansion coefficient than steel, so that the heating of the sample tends to keep it taut. Above 300°C , however, vanadium rapidly loses its strength, and the weight of the molten lead (mp 327°C) causes it to bulge if unsupported. To help prevent this, three steel support ribs were placed on each side of the sample. To make the sample frame and the support ribs look as black as possible to neutrons, they were painted with gadolinium-oxide powder. The paint was made by mixing the powder with an aluminum-base, high-temperature furnace paint as a binder. An empty sample holder of identical construction was used to obtain background corrections. The sample temperature was maintained at $352 \pm 5^\circ\text{C}$. The measured sample transmission, when oriented at 45° to the incident beam, was 0.91 at 0.02 eV.

TABLE I. Velocity-selector resolution for elastic scattering.

E_0 (eV)	Δt (μsec)	$\Delta t/t_0$	$\Delta E/E_0$	ΔE (meV)	$\Delta\beta = \Delta E/k_B T$
0.0149	22.7	0.0170	0.0340	0.506	0.0094
0.0170	21.7	0.0173	0.0346	0.588	0.0109
0.0200	22.0	0.0191	0.0382	0.764	0.0142

Data runs were taken at incident energies of 0.0149, 0.0170, and 0.0200 eV with an analyzer channel width of $10 \mu\text{sec}$. At these energies the chopper system has a low transmission for 12 000 rpm operation with the 116.6-cm radius slits available. The choppers and the collimators were therefore both run at 7500 rpm to increase the transmission. In spite of the slower chopping speed, the energy resolution was satisfactory. The resolution is computed from the time spread of the transmitted beam as measured at the beam monitor located at the same distance from the sample as the scattered-neutron detectors. This gives the resolution for elastic scattering. The fractional time resolution is $\Delta t/t_0$, where t_0 is the sample-to-detector time of flight, and $\Delta t = 2\sigma$, where σ^2 is the variance of the burst at the detector. Table I gives the values for the energy resolution.

B. Helium Flight Path and the Effects of Air Scattering

To reduce the effects of air scattering, a helium-filled, cadmium-lined flight path was constructed and installed for this experiment, as shown in Fig. 2. The detectors are mounted in cadmium-lined aluminum boxes which are clamped to the outside of the flight path. The entire 51-cm-high arc from 15° to 90° at the detectors is covered with a single 0.0127-cm thick aluminum window.

Gas-scattering contributions are mainly due to scattering of the transmitted forward beam by the column of gas downstream from the sample. Because of the finite sample size used, collimation of this region cannot be done close to the target, so that an uncollimated region of gas exists just forward of the sample. In this experiment this gas column was 50 cm long.

A comparison of the effect on the scattering from liquid lead of having helium or air in the flight path has been made, other conditions being identical. Figure 3 shows a comparison of these effects at scattering angles of 15° , 20° , and 25° . The effects of air are quite marked at small angles for this energy, but decrease with increasing scattering angle and at an angle of 40° are no longer observable. The relative contribution of gas scattering is large at small angles simply because the lead scattering cross section is very small here while the gas cross section is largest. As the scattering angle increases, however, the lead cross section increases by a factor of ~ 100 while the gas cross section decreases. In Figs. 3(a) and 3(b) are shown sample and background raw data for the lead sample taken in

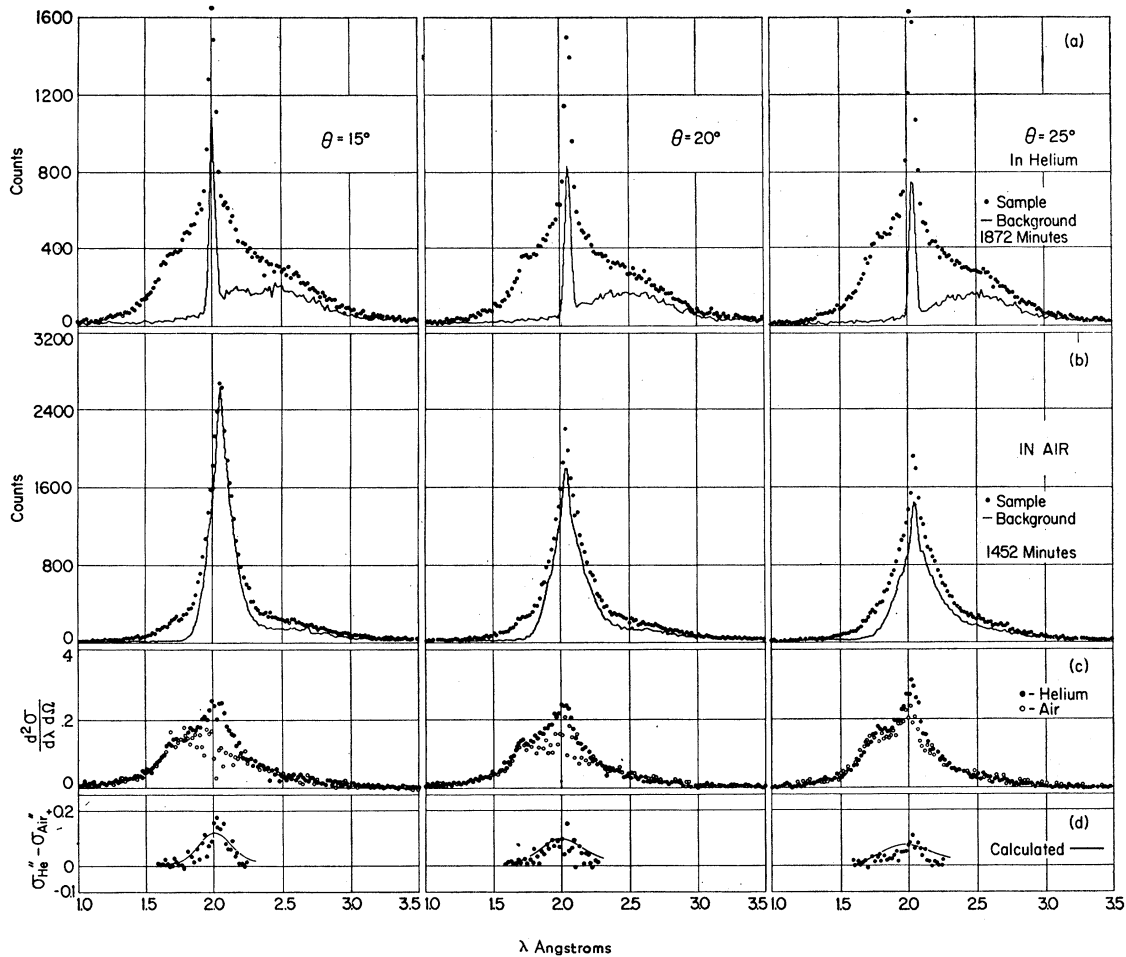


FIG. 3. Comparison of the scattering from liquid lead in air and in helium flight paths: (a) sample and background data in helium, (b) sample and background data in air, (c) partial differential cross sections of lead in helium and air, and (d) difference of the partial differential cross sections of lead obtained in helium and in air. The solid curve is from an ideal-gas calculation.

both helium and air. Note that these were taken with different running times so that the counting rates should not be directly compared. However, the background due to air scattering is quite marked, comprising most of the observed scattering but decreases in relative magnitude with increasing angle. In contrast, the background with helium in is quite small. The sharp spike appearing at the incident wavelength in the data taken in helium is due to the elastic incoherent scattering from the vanadium cover foils of the empty sample holder. In both cases there is observed a low, broad hump on the longer wavelength side in both sample and background data. This arises because the rotating collimators were run at the same speed as the choppers and pass two bursts for each chopper burst. The background maxima are caused by the 180° opening of the first collimator. Figure 3(c) shows the resulting cross section $d^2\sigma/d\lambda d\Omega$ obtained from the data of Figs. 3(a) and 3(b). The air clearly reduces the observed cross section for small wavelength changes. In Fig. 3d is plotted the difference between the cross

section for liquid lead observed in helium and that observed in air. Also shown is a calculated curve of this difference. This smooth curve is calculated assuming ideal-gas scattering from the downstream column of gas, and that the scattering takes place as if the whole gas column were located at the sample. This is surely not so, since this uncollimated column is ≈ 0.5 m long, and this assumption gives rise to errors in the assumed flight-path distance and therefore to wavelength errors. However, the calculated curve is in agreement with the observed cross-section difference. It is seen, however, that the agreement becomes poorer with increasing angle and wavelength. This is believed to be due to the above-mentioned path length errors. Since the main experiment was performed in helium, the scattering from this should also have an effect compared to what would be observed in a vacuum. As compared to a vacuum, a similar calculation shows that the maximum error due to scattering in the helium would not exceed $\sim 1.3\%$. No correction for this has been applied to the data.

C. Background Corrections and Velocity-Selector Calibration

Since absolute cross sections are measured in this experiment and from these a "one-phonon" contribution is extracted, several corrections to the data are necessary. The most important subtractive corrections are: (a) background, (b) multiphonon effects, and (c) multiple scattering. We confine our attention here to the background correction; the last two corrections are discussed in Sec. VIA.

The background data were run for the same length of time as the sample, generally from 2000 to 3000 min each by cycling at 10-min intervals. The background data are corrected, if necessary, to give the same counting rate as the sample at both long and short times of flight where it is assumed that no significant inelastic scattering remains. Figure 4(a) shows a representative plot of sample and background data, and Fig. 4(b) illustrates the counting-rate differences obtained from Fig. 4(a) averaged over several channels. The dotted line in Fig. 4(b) shows the correction that is then added to the background. These corrections to the background are generally very small, being of the order of 10–20 counts out of several thousands at the main peak.

The velocity selector, after moving it to the new beam hole, was calibrated for this experiment using methane as a standard. A room-temperature sample of methane gas [56 psi (gauge)] was run at 0.025 eV. The scattering law from this run was then compared with that obtained from earlier methane experiments¹² and with the methane calculations of Griffing.¹³

IV. EXPERIMENTAL RESULTS

A. Cross Sections

The experimental data after correction for background and counter efficiency were converted to the partial differential cross section and to the scattering law in the form of the reduced partial differential cross section $S_R(\kappa, \hbar\omega)$:

$$d^2\sigma/dEd\Omega = (E/E_0)^{1/2} e^{-\beta/2} S_R(\kappa, \hbar\omega), \quad (1)$$

$$\beta = (E - E_0)/k_\beta T = \hbar\omega/k_\beta T, \quad (2a)$$

$$\kappa = \mathbf{k} - \mathbf{k}_0, \quad (2b)$$

where E_0 , E and \mathbf{k}_0 , \mathbf{k} are the incident and scattered-neutron energies and wave vectors, respectively. The scattering law $S_R(\kappa, \hbar\omega)$ has the dimensions of barns/[eV steradian atom) and is an even function of the energy transfer $\hbar\omega$. Also, since the sample is isotropic, $S_R(\kappa, \hbar\omega)$ depends on κ only through its magnitude $|\kappa| = \kappa$.

Figure 5 shows representative plots of the partial differential cross section for an incident energy of

¹² P. D. Randolph, R. M. Brugger, K. A. Strong, and R. E. Schmunk, *Phys. Rev.* **124**, 460 (1961).

¹³ G. W. Griffing, in *Inelastic Scattering of Neutrons in Solids and Liquids* (International Atomic Energy Agency, Vienna, 1963), Vol. I, p. 435.

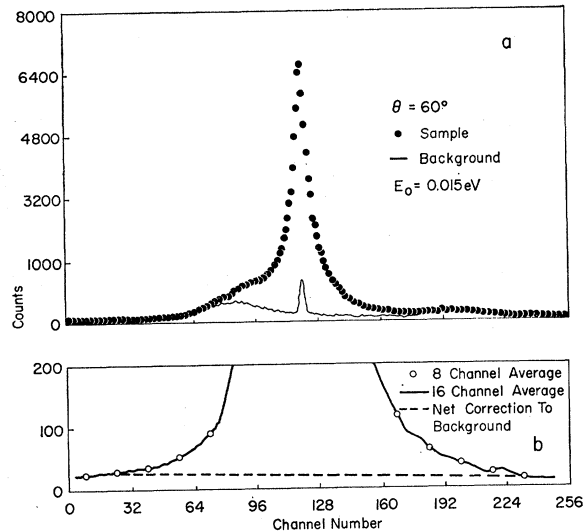


FIG. 4. Background corrections: (a) raw data for liquid lead at 60° scattering angle, (b) average over 8 and 16 channels of the "sample" minus "open" difference in counting rate. The dotted line shows the correction to the background obtained from the 16 channel average.

0.0170 eV. These data are also typical of the 0.015- and 0.020-eV runs. Also shown is the spectrum of the incident beam. The inelastic scattering is quite marked, especially for small scattering angles, where a definite structure is observed. This structure arises from the excitation of "collective modes" in the liquid and has also been observed in liquid lead by Cocking and Egelstaff⁴ using very cold neutrons. From the energy and momentum transfer at the peaks or breaks in the structure, they have obtained a dispersion curve for "quasi-phonons" in the liquid.

One also observes that a slight structure remains in the inelastic scattering at short wavelengths even for larger angles. It is most clearly seen at angles from 55° through 75°. For the other angles, corresponding to peaks in the diffraction pattern, the maximum cross section is so large that very little or no structure can be seen in the inelastic scattering. This structure arises from single and multiple excitation of the collective vibrations in the liquid. It is this region of the inelastic scattering that we shall be concerned with.

B. Scattering Law

The scattering law data $S_R(\kappa, \hbar\omega)$ are shown in Fig. 6 for various fixed values of the energy transfer. This comprises data from the 0.015-, 0.017-, and 0.020-eV runs. No normalization has been applied to these data. The error flags shown are due to counting statistics only.

κ -dependent structure for small energy transfers is quite marked. This has already been observed in liquid sodium¹ but was less pronounced, since sodium is a partially incoherent scatterer. The structure is also

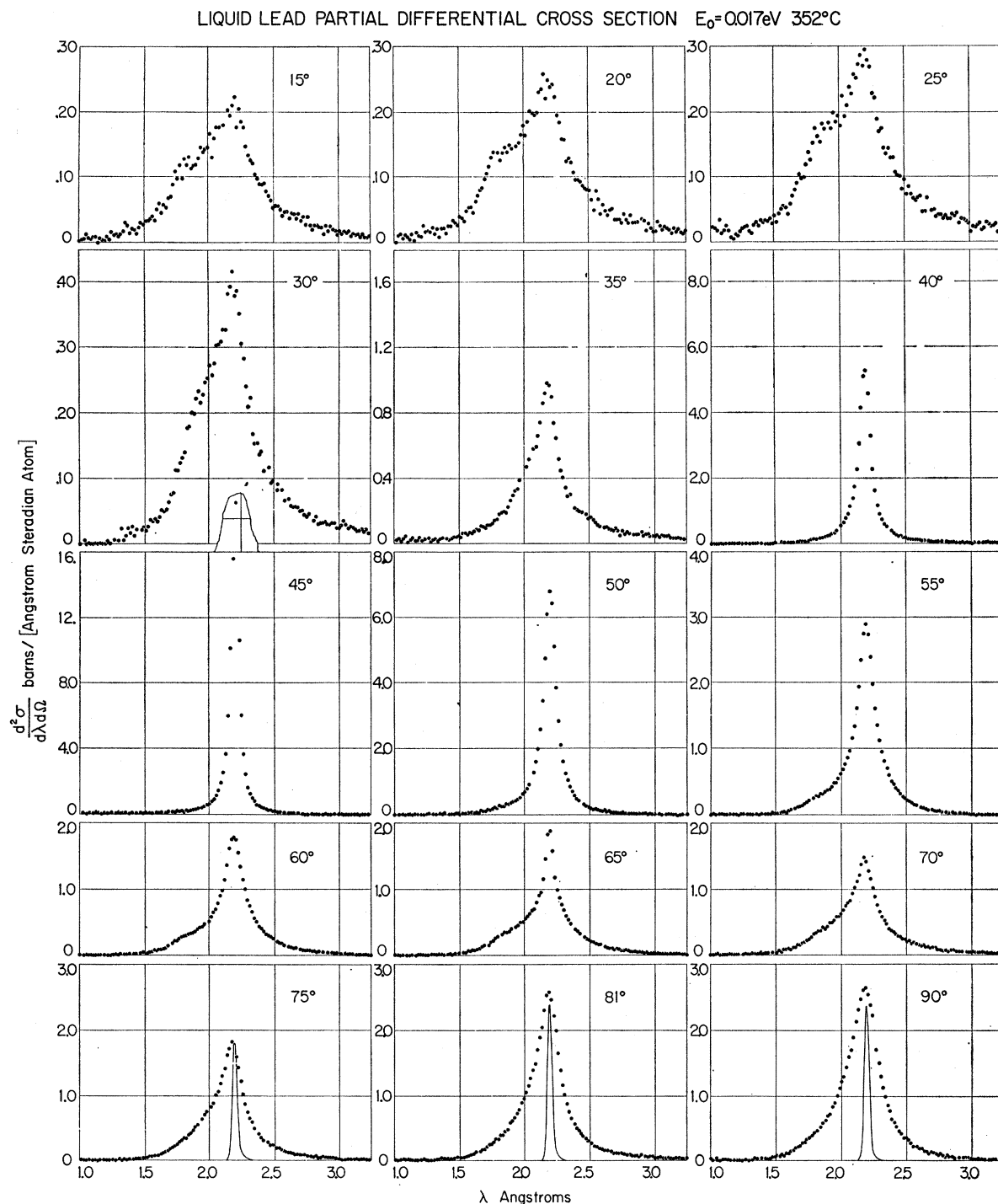


Fig. 5. Partial differential cross section for scattering from liquid lead as a function of scattered-neutron wave length.

more accurately defined in this experiment due to higher intensity, and improved angular and energy resolution. At zero-energy transfer the cross section varies by a factor of 10^2 in going from $\kappa=1.0 \text{ \AA}^{-1}$ to 2.2 \AA^{-1} , and at $\kappa=2.2 \text{ \AA}^{-1}$ the observed cross section changes by three orders of magnitude in going from 0-

to 16-meV energy transfer. The main structure, which is characteristic of the first two peaks in the diffraction pattern (see Fig. 8) damps out fairly quickly with increasing energy transfer. It is also seen that the principal maximum becomes broader and shifts to larger κ as β increases. As the energy transfer con-

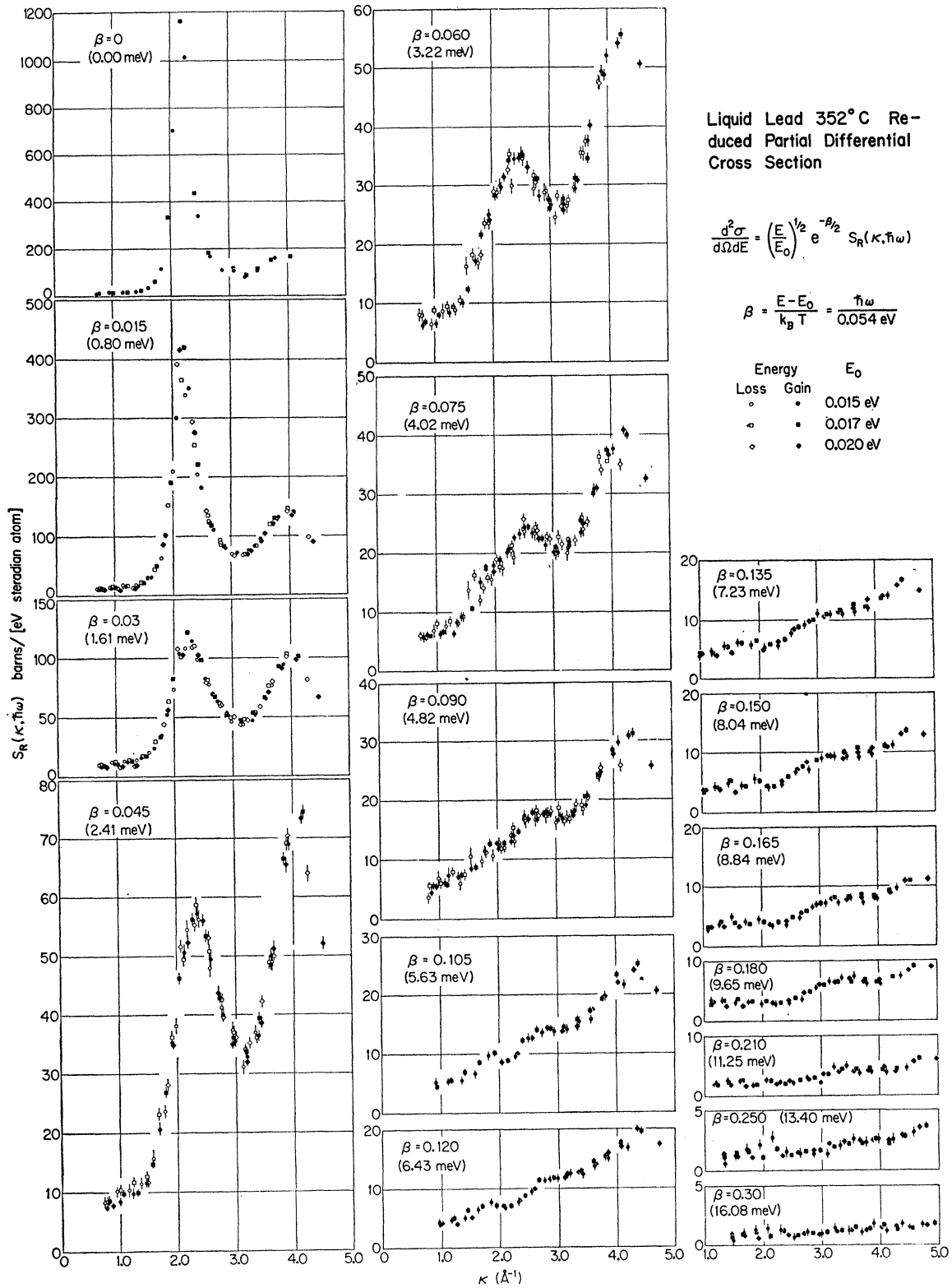


FIG. 6. Scattering-law data for liquid lead showing the combined results at three incident energies. The error flags shown are due to counting statistics only.

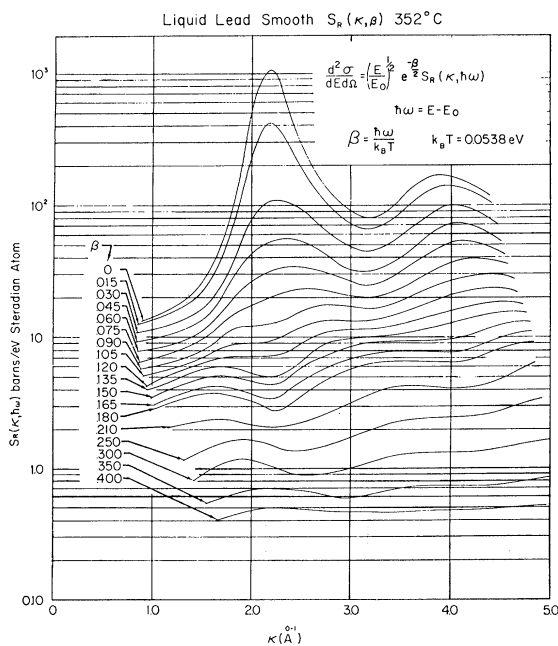


FIG. 7. Smooth-curve scattering law for liquid lead obtained from the data of Fig. 6.

tinues to increase, some structure still remains though it is smaller. The most noticeable feature at the larger energy transfers ($\beta \gtrsim 0.09$) is the appearance of another broad secondary maximum at $\kappa < 2.2 \text{ \AA}^{-1}$. This shifts gradually to smaller κ values. In Fig. 7 are shown smooth curves of the scattering law. These are hand-drawn curves through the data points, and conveniently illustrate on one graph the changes in the structure of the scattering law. The appearance of the maxima on either side of $\kappa = 2.2 \text{ \AA}^{-1}$ is another manifestation of the quasi-phonon excitation in the liquid and is discussed in Sec. VIB.

C. Diffraction Pattern

The observed scattering law has been used to obtain the diffraction pattern $1 + \Gamma(\kappa)$ from this experiment. The expression for this is given by

$$\frac{\sigma_{\text{coh}}}{\sigma_b} [1 + \Gamma(\kappa)] = \frac{4\pi k_B T}{\sigma_b} 2 \int_0^\infty \cosh(\beta/2) S_R(\kappa, \beta) d\beta, \quad (3)$$

where σ_{coh} and σ_b are the coherent and bound-atom total scattering cross sections, respectively, for both of which the value of 11.4 b has been used. This expression has been evaluated using the smooth-curve scattering law of Fig. 7. In Fig. 8 the results (not normalized) are shown together with those of Kaplow, Strong, and Averback¹⁴ obtained from x-ray diffraction, and those of Sharrah, Petz, and Kruh¹⁵ obtained from neutron-

¹⁴ R. Kaplow, S. L. Strong, and B. L. Averback, Phys. Rev. 138, A1336 (1965).

¹⁵ P. C. Sharrah, J. I. Petz, and R. F. Kruh, J. Chem. Phys. 32, 241 (1960).

diffraction studies. The results of this experiment agree rather well with the neutron diffraction results of Sharrah *et al.* There are significant differences between the x-ray and neutron results, as is evident from the figure. At small values of κ both neutron experiments give high values. This discrepancy between the neutron and x-ray results at small κ is primarily due to the presence of multiple scattering, both elastic and inelastic, in the neutron experiments. The evidence for multiple scattering in this experiment is discussed in more detail in Sec. VIA. The difference in magnitudes of the main diffraction peak probably arises from the finite spread in κ used in this experiment, but whether this would account for all the discrepancy is not known. In the range $\kappa \lesssim 1.8 \text{ \AA}^{-1}$ the x-ray results are not very reliable¹⁶ and therefore have been fitted smoothly to other x-ray results of Sharrah *et al.*¹⁵ We shall need accurate values of the diffraction pattern in the region of the main maximum in order to compare the inelastic scattering data with the QC model. In order to determine which diffraction pattern is more reliable (near the diffraction peak), we have used the criterion recently suggested by Rahman¹⁷ and found that the x-ray results of Kaplow *et al.*¹⁴ satisfy the criterion better than either set of neutron results.

D. Multiphonon and Multiple Scattering Effects

The presence of collective modes, if any, will manifest themselves most clearly in the "one-phonon" part of the scattering law. We have therefore to correct for multiphonon effects and multiple scattering.

Since for liquid lead the "Debye temperature" is $\Theta_D \lesssim 100^\circ\text{K}$ and the sample temperature is 625°K , multiphonon contributions are expected to be appreciable even though the momentum transfers of interest here are not very large. The multiphonon contributions

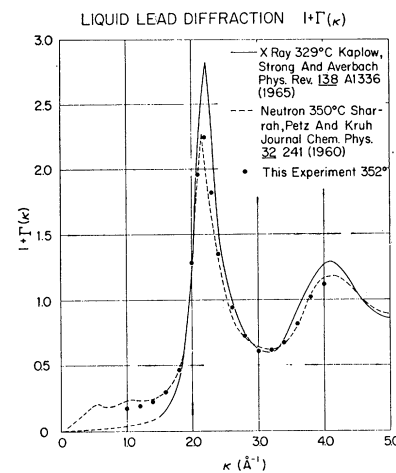


FIG. 8. Comparison of the diffraction pattern obtained in this experiment by integration of the scattering law, with the x-ray data of Kaplow *et al.* (Ref. 14) and the neutron diffraction data of Sharrah *et al.* (Ref. 15).

¹⁶ R. Kaplow (private communication).

¹⁷ A. Rahman, J. Chem. Phys. 42, 3540 (1965).

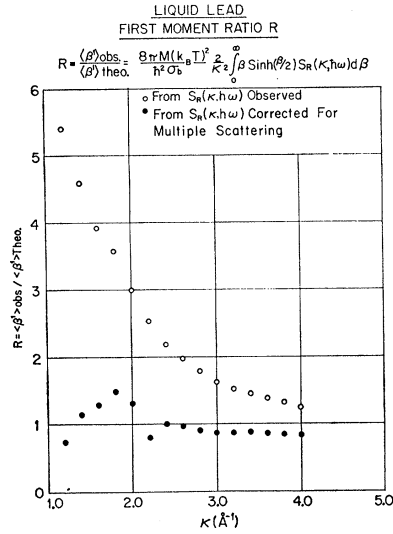


FIG. 9. The ratio R of the observed to the theoretical first-moment of the scattering law for liquid lead.

were evaluated using the LEAP¹⁸ program, which is based on the incoherent harmonic approximation. Physically, it is reasonable to assume that this approximation is fairly good, and that it is so has been demonstrated by Larsson *et al.*¹⁹ in both polycrystalline and liquid aluminum. It has also been used extensively in making multiphonon corrections for such coherent materials as polycrystalline BeO, Be,²⁰ and graphite.²¹ To make such a calculation for a solid, one needs the frequency distribution $f(\omega)$ of the normal modes. The multiphonon contribution is, however, rather insensitive to the precise shape of this function.²²

For a liquid, $f(\omega)$ is to be replaced by the Fourier transform of the velocity autocorrelation function.²³ Since this function is not known from experiments, we have assumed the following simple form for the vibratory modes⁶:

$$f(\omega) = (4/\omega_m^3)\omega^2 e^{-2\omega/\omega_m}, \quad (4)$$

and $f(\omega)$ is normalized to unity. The maximum of $f(\omega)$ occurs at $\omega = \omega_m$, which is taken as a parameter. This form assumes that the area under the diffusive part of $f(\omega)$ is small compared to the total area. Since we are interested here in energy transfers large compared to those involved in diffusive motion, the diffusive part of $f(\omega)$ is not of much importance.

¹⁸ J. D. Macdougall, Brookhaven National Laboratory Report No. BNL-719 (U. S. Government Printing and Publishing Office, Washington, D. C., 1962), Vol. I, p. 121.

¹⁹ K. E. Larsson, U. Dahlborg, and D. Jovic, in *Inelastic Scattering of Neutrons in Solids and Liquids* (International Atomic Energy Agency, Vienna, 1965), Vol. II, p. 117.

²⁰ R. N. Sinclair, in *Inelastic Scattering of Neutron in Solids and Liquids*, (International Atomic Energy Agency, Vienna, 1963), Vol. II, p. 199.

²¹ B. C. Haywood and I. M. Thorson, in *Inelastic Scattering of Neutrons in Solids and Liquids* (International Atomic Energy Agency, Vienna, 1963), Vol. II, p. 111.

²² A. Sjölander, Ark. Fys. 17, 315 (1958).

²³ A. Rahman, K. S. Singwi, and A. Sjölander, Phys. Rev. 126, 986 (1962).

Calculations of the multiphonon contributions were made using LEAP for four different values of ω_m corresponding to temperatures T_m of 50, 60, 70, and 80° K, and a value of $T_m = 70^\circ\text{K}$ was found to give the best results.

We turn now to a discussion of multiple scattering. The strongest evidence for the presence of multiple scattering comes from evaluating the first moment of the observed scattering law with respect to the energy transfer. In terms of the dimensionless variable β , the first moment is given by²³:

$$\langle \beta^1 \rangle \equiv \frac{4\pi k_B T}{\sigma_b} 2 \int_0^\infty \beta \sinh(\beta/2) S_R(\kappa, \beta) d\beta = \frac{\hbar^2 \kappa^2}{2M k_B T}, \quad (5)$$

where M is the mass of the scattering atom. The above sum rule is valid for any system that is reflection invariant and in which there are no velocity-dependent forces. From Eq. (5) it follows that the ratio R of the observed first moment to the theoretical value $\hbar^2 \kappa^2 / 2M k_B T$ should be unity.

Measurements of R using the uncorrected smooth scattering law of Fig. 7 are shown in Fig. 9. The ratio is seen to be a factor of almost 6 too large at small κ and decreases to a factor of ~ 1.3 at $\kappa = 4.0 \text{ \AA}^{-1}$. Thus there are extraneous contributions present in the scattering law. That these arise from multiple scattering is evident from some earlier work on aluminum powder.²⁴ In that experiment scattering-law measurements were made on a sample of aluminum powder in the form of a stack of 18 parallel compressed blocks (transmission 0.87). One set of runs was made with cadmium spacers between the blocks to reduce multiple scattering perpendicular to the scattering plane, then another set of runs was made without the spacers. The moment ratio R was then obtained for both cases. Figure 10 shows this moment ratio for aluminum. From the figure it is apparent that, if not all, a large part of the moment discrepancy arises from multiple scattering.

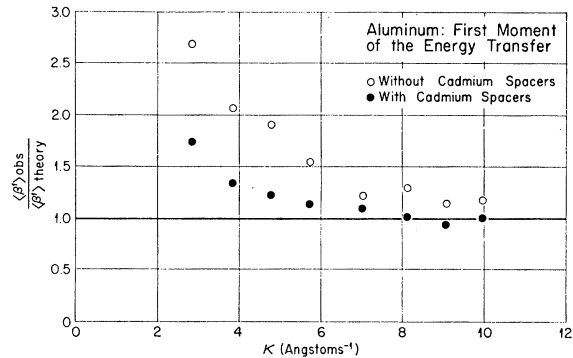


FIG. 10. First-moment ratio R for aluminum powder showing the effect of introducing cadmium spacers to reduce multiple scattering

²⁴ R. M. Brugger and P. D. Randolph, U. S. Atomic Energy Commission Report No. IDO-17063 1965 (unpublished).

Presumably, the same multiple-scattering effects are responsible for the moment discrepancy in liquid lead. In general, multiple scattering depends not only on the energy transfer but also on the momentum transfer. At present there exists no accurate method of making multiple-inelastic-scattering corrections in coherent materials. We have made a crude correction for this effect by assuming that all the observed scattering at $\kappa \leq 1.0 \text{ \AA}^{-1}$ for all energy transfer arises from multiple scattering. A similar assumption was also made by Brockhouse and Pope.²⁵ The function $S_{R,\text{obs}}(1.0, \hbar\omega)$ is then subtracted from the observed scattering law for all κ values. In Fig. 9 solid points show the corrected first moment. The multiple-scattering correction thus results in a considerable improvement in the moment ratio. The remaining discrepancy is probably due to the κ -dependent nature of the multiple scattering, which, since it is unknown, we have not accounted for. The above assumption that all the observed scattering below $\kappa = 1.0 \text{ \AA}^{-1}$ is due to multiple scattering would also bring the observed neutron structure factor $1 + \Gamma(\kappa)$ (Fig. 8) for low values of κ more nearly in agreement with x-ray results.

V. THEORETICAL MODEL

The QC model with which the data of this experiment are compared is described in detail in Refs. 7 and 8, and we give here only a brief outline of it, together with the necessary formulas used in computations. The intermediate scattering function may be written

$$F(\mathbf{\kappa}, t) = F_S(\mathbf{\kappa}, t)[1 + \Gamma(\mathbf{\kappa})] + H(\mathbf{\kappa}, t), \quad (6)$$

where

$$H(\mathbf{\kappa}, t) = \frac{1}{N} \sum_{l \neq m}^{<R} \langle \exp[i\mathbf{\kappa} \cdot \mathbf{R}_l(0)] \exp[-i\mathbf{\kappa} \cdot \mathbf{R}_m(t)] \rangle_T \\ - \frac{1}{N} \sum_{l \neq m}^{<R} \langle \exp[i\mathbf{\kappa} \cdot \mathbf{R}_l(0)] \exp[-i\mathbf{\kappa} \cdot \mathbf{R}_m(0)] \rangle_T \\ \times \langle \exp[i\mathbf{\kappa} \cdot \mathbf{R}_m(0)] \exp[-i\mathbf{\kappa} \cdot \mathbf{R}_m(t)] \rangle_T. \quad (7)$$

$\mathbf{R}_l(0)$ and $\mathbf{R}_m(t)$ are the Heisenberg position operators for the l th atom at time 0 and the m th atom at time t , respectively. The sum in Eq. (7) is over all atoms which lie inside a sphere of radius R with atom l at the center. This sum is to be understood in the following sense:

$$\frac{1}{N} \sum_{l \neq m}^R \langle \exp[i\mathbf{\kappa} \cdot \mathbf{R}_l(0)] \exp[-i\mathbf{\kappa} \cdot \mathbf{R}_m(0)] \rangle_T \\ = \int e^{i\mathbf{\kappa} \cdot \mathbf{r}} g(\mathbf{r}) \exp(-|\mathbf{r}|^2/R^2) d\mathbf{r}, \quad (8)$$

where $\hbar\mathbf{\kappa}$ is the momentum transfer and $g(\mathbf{r})$ is the static pair correlation function. In writing $F(\mathbf{\kappa}, t)$ in Eq. (6)

it is assumed that the convolution approximation²⁶ holds for all atoms whose separation is greater than a certain distance R . The correction $H(\mathbf{\kappa}, t)$ to the convolution approximation, which is supposed to take care of the correlated motion of atoms inside R at short times, was evaluated as if the liquid behaved as a quasi-harmonic solid. The inelastic-partial-differential scattering cross section in "one-phonon" approximation is then given by⁸

$$\frac{d^2\sigma}{dE d\Omega} = \left(\frac{E}{E_0}\right)^{1/2} \exp\left(-\frac{\hbar\omega}{2k_B T}\right) S_{R,\text{coh}}^{1\text{ph}}(\mathbf{\kappa}, \hbar\omega), \quad (9)$$

where

$$S_{R,\text{coh}}^{1\text{ph}}(\mathbf{\kappa}, \hbar\omega) = S_{\text{inc}}^{1\text{ph}}(\mathbf{\kappa}, \hbar\omega) [1 + \Gamma(\mathbf{\kappa}) \\ + \text{sech}\left(\frac{\hbar\omega}{2k_B T}\right) \omega^2 / 6C^2 \times L(R, \kappa, q)], \quad (10)$$

and

$$S_{\text{inc}}^{1\text{ph}}(\mathbf{\kappa}, \hbar\omega) = \frac{\sigma_{\text{coh}}}{4\pi} \exp(-\mathbf{\kappa}^2 a) \coth\left(\frac{\hbar\omega}{2k_B T}\right) \\ \times \frac{\kappa^2 \hbar\omega}{4M} \frac{f(\omega)}{\omega^2}, \quad (11)$$

$$L(R, \kappa, q) = \frac{3R}{q^2 \kappa \sqrt{\pi}} \int_0^\infty k \Gamma(\kappa) dk \frac{1}{2q} \\ \times \int_{-q}^q \left\{ \left[\exp\left(\frac{-R^2}{4}(k - \kappa + x)^2\right) \right. \right. \\ \left. \left. - \exp\left(\frac{-R^2}{4}(\kappa + k + x)^2\right) \right] - \left[\exp\left(\frac{-R^2}{4}(\kappa - k)^2\right) \right. \right. \\ \left. \left. - \exp\left(\frac{-R^2}{4}(k + \kappa)^2\right) \right] \right\} dx. \quad (12)$$

In these equations R is the coherence parameter defined in Eq. (8), q is the magnitude "quasiphonon" wave vector, $\Gamma(\kappa)$ is the Fourier transform of the static-pair correlation function $g(\mathbf{r})$, and $\exp(-\mathbf{\kappa}^2 a)$ is the Debye-Waller factor. $f(\omega)$ is the frequency spectrum given by the Fourier transform of the velocity autocorrelation function, for which we have used the form given in Eq. (4), C is the velocity of sound and σ_{coh} is the bound-atom total coherent scattering cross section.

A few remarks about Eq. (10) are worth making. This formula, as we might have expected, is of the same form as the one-phonon scattering law for a polycrystalline coherent harmonic solid, but with two modifications: (a) the usual frequency distribution function $f(\omega)$ for a solid has been replaced by the Fourier transform of the velocity autocorrelation function; and (b) the polycrystalline structure factor, which involves a sum over the reciprocal lattice vectors, has been re-

²⁵ B. N. Brockhouse and N. K. Pope, Phys. Rev. Letters 3, 259 (1959).

²⁶ G. H. Vineyard, Phys. Rev. 110, 999 (1958).

placed by the term within the square bracket of Eq. (10), which we shall henceforth call $Z_{\text{liq}}(\mathbf{\kappa}, q)$. Using the momentum-conservation condition $\mathbf{\kappa} + \mathbf{q} = 2\pi\boldsymbol{\tau}$ and in the limit of small \mathbf{q} , it was shown in the Appendix of Ref. 8 that the polycrystalline structure factor is identical to our $Z_{\text{liq}}(\mathbf{\kappa}, q)$. It is important to note that formula (10) was derived without any assumption of the existence of a reciprocal lattice vector. We might refer to $Z_{\text{liq}}(\mathbf{\kappa}, q)$ as the dynamical structure factor of a liquid. For a fixed value of the energy transfer, any manifestation characteristic of collective behavior in $S_{R\text{coh}}^{1\text{ph}}(\mathbf{\kappa}, \hbar\omega)$ as a function of κ depends only on $Z_{\text{liq}}(\mathbf{\kappa}, q)$ and is independent of the details of $f(\omega)$. None of the κ -dependent structure or peaks arise from $S_{\text{inc}}^{1\text{ph}}(\mathbf{\kappa}, \hbar\omega)$ since its κ dependence is smooth, i.e., $\sim \kappa^2 \exp(-\kappa^2 a)$.

The dynamical structure factor of a solid gives rise to discontinuities in the scattering cross section corresponding to the condition

$$|\mathbf{\kappa} - \mathbf{q}| < 2\pi|\boldsymbol{\tau}| < |\mathbf{\kappa} + \mathbf{q}|.$$

Our function $Z_{\text{liq}}(\mathbf{\kappa}, q)$ does the same thing, but the discontinuities are smoothed out—a fact in agreement with observation. From the observed cross section one has to obtain the function $Z_{\text{liq}}(\mathbf{\kappa}, q)$ or more precisely that term which contains the function $L(R, \kappa, q)$ to extract the collective behavior in a liquid.

VI. COMPARISON WITH THE MODEL AND DISCUSSION

To make a comparison of the QC model with the experiment we need to know the one-phonon part of the scattering law. The latter is evaluated by subtracting from the observed scattering law the multiphonon and multiple-scattering contributions discussed earlier, that is

$$S_{\text{coh, obs}}^{1\text{ph}}(\mathbf{\kappa}, \hbar\omega) = S_{\text{obs}}^{\text{tot}}(\mathbf{\kappa}, \hbar\omega) - S^{\text{M.S.}}(\mathbf{\kappa}, \hbar\omega) - S^{\text{m.ph.}}(\mathbf{\kappa}, \hbar\omega).$$

The theoretical scattering law was calculated from Eqs. (10) and (11) for three values of T_m , 60, 70, and 80°K, using $f(\omega)$ given by Eq. (4). In making this calculation we have to know the magnitude of the phonon wave number q corresponding to the energy transfer $\hbar\omega$; that is, we have to have a dispersion relation. We have made the simplest assumption of a linear dispersion law with the velocity of sound $C = 1.77 \times 10^5$ cm/sec (as obtained by Gordon from ultrasonic measurements at 350°C).²⁷ As we shall see later, the choice of this dispersion relation and sound velocity is a reasonable one. In view of the approximation made in the model and the limited accuracy of these experimental corrections, the use of a more complicated dispersion law is not warranted. In making the calculation of Eq. (10), the Debye-Waller factor

was obtained from the LEAP calculation; and we have taken the coherence radius R to be 20 Å. In evaluating the function $L(R, \kappa, q)$, the values used for $1 + \Gamma(\kappa)$ were those of Kaplow *et al.*,¹⁴ corrected at the low κ values.

In Fig. 11 we have plotted the scattering law $S_R(\mathbf{\kappa}, \hbar\omega)$ as a function of κ for various values of β for $T_m = 70^\circ\text{K}$. From an inspection of this figure one can make the following observations about $S_{R\text{obs}}^{1\text{ph}}(\mathbf{\kappa}, \hbar\omega)$: (a) For $\beta = 0.075$ the observed $S_R^{1\text{ph}}(\kappa, \hbar\omega)$ has a structure very similar to that of $1 + \Gamma(\kappa)$ except that there are slight indications of the development of a broad maximum on either side of $\kappa \cong 2.2 \text{ \AA}^{-1}$; (b) as the energy transfer increases, these maxima become more pronounced and are clearly seen; (c) the positions of these maxima shift in κ with increasing β ; and (d) the one-phonon cross section has a minimum around $\kappa = 2.2 \text{ \AA}^{-1}$ for $\beta > 0.090$. For $\beta \gtrsim 0.150$ the nature of the cross section is shown by the smooth curves of Fig. 7. However, the cross section has fallen to such low values that $S_{R\text{obs}}^{1\text{ph}}(\mathbf{\kappa}, \hbar\omega)$ is not very reliable; and hence we have not considered these β values in our interpretation.

The dashed curves in Fig. 11 show the calculated one-phonon scattering law using the convolution approximation. These curves do not exhibit any of the subsidiary structure that is present in the experimental curves. Further, the main diffraction peak at $\kappa = 2.2 \text{ \AA}^{-1}$ continues to persist; and the value of the cross section at the peak is much higher than the observed values.

The solid curves exhibit the calculated scattering law based on the model under discussion. These curves do show the subsidiary maxima, though not as pronounced as in the experiment, and they also shift with increasing values of β . The value of the calculated cross section at $\kappa = 2.2 \text{ \AA}^{-1}$ is higher than observed but definitely lower than given by the convolution approximation. In fact, there is a minimum in the value of the observed cross section at the above value of κ , whereas the model has a maximum. We discuss this discrepancy in the discussion of $L(R, \kappa, q)$.

The coherent inelastic effects are small and are entirely contained in the term with $L(R, \kappa, q)$ in Eq. (10). In order to bring out these effects more vividly we have plotted in Fig. 12 the observed $L(R, \kappa, q)$ function. Experimental values for the latter are obtained from Eqs. (10) and (11) using for the left-hand side of Eq. (10) the observed values of $S_{R\text{coh}}^{1\text{ph}}(\kappa, \hbar\omega)$. The errors shown on the experimental points represent counting statistics only. The uncertainty in the κ values is not shown but is $\Delta\kappa \cong \pm 0.05 \text{ \AA}^{-1}$. The solid curves represent the calculated values of the function $L(R, \kappa, q)$. Figure 12 exhibits in a striking fashion the more important features of the dynamical structure factor $Z_{\text{liq}}(\mathbf{\kappa}, q)$. We may note the following features of the L function: (a) It has a deep minimum at $\kappa = 2.2 \text{ \AA}^{-1}$ flanked by a subsidiary maximum on each side; (b) with increasing values of β the minimum becomes both shallower and broader and so do the subsidiary maxima; (c) the maxima move

²⁷ R. B. Gordon, *Acta Met.* 7, 1 (1959).

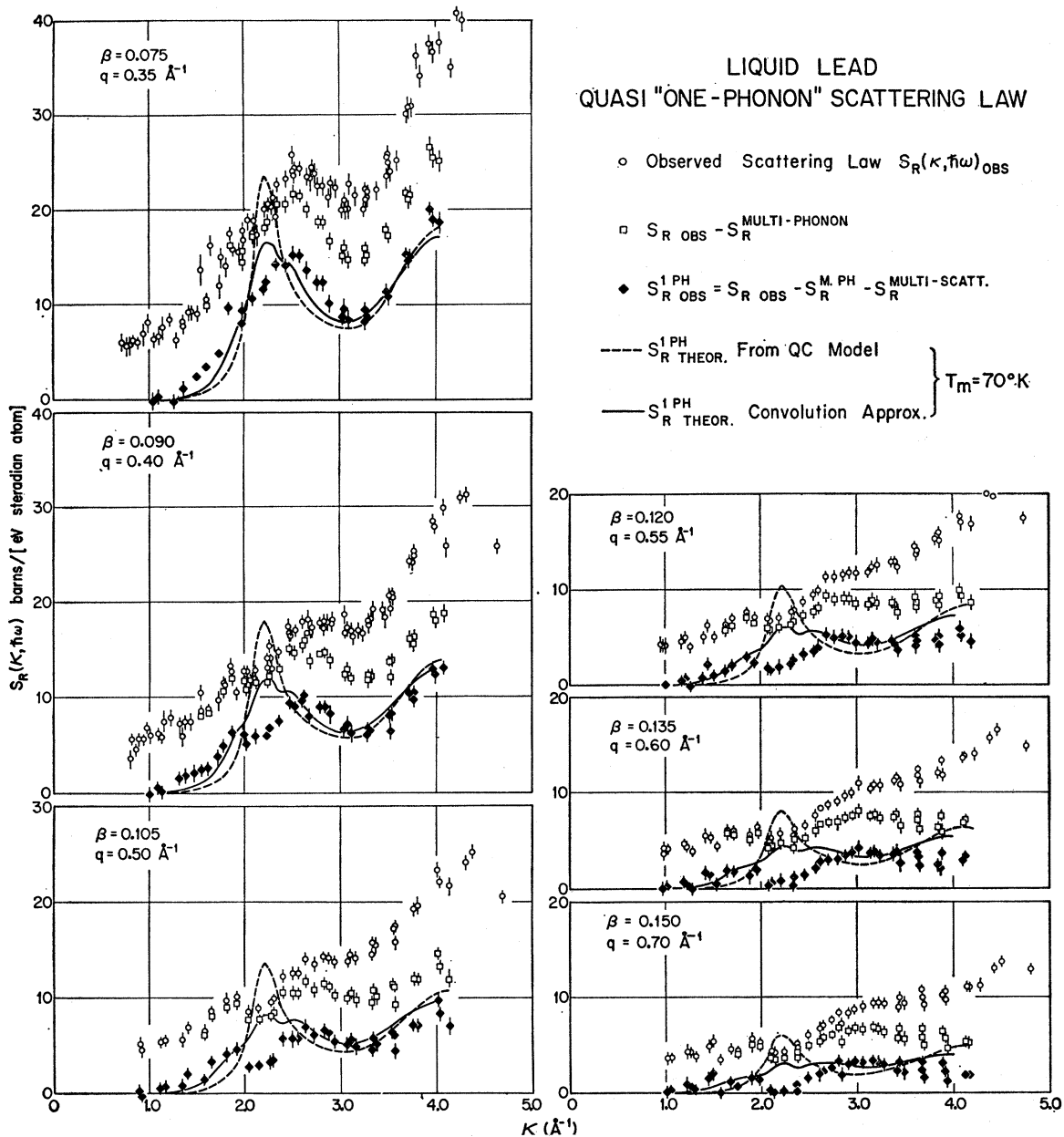


FIG. 11. Comparison of the observed liquid-lead "one-phonon" scattering law with that given by the model and the convolution approximation.

away from $\kappa = 2.2 \text{ \AA}^{-1}$ with increasing β ; and (d) the left-hand maximum is more pronounced than the right-hand one and higher. All these above-mentioned features are present in the experimental L function.

If the convolution approximation were valid in the range of κ values considered here, the experimental points would have fluctuated randomly about $L=0$, which indeed is not the case. Thus the model under consideration does have the essential features seen in the experiment. Even the quantitative agreement with the experiment is surprisingly good in spite of the crudeness of the model and the uncertainties in the

corrections to the observed total scattering law. The main quantitative discrepancies are in the depth of the minimum for all β values and in the height of the left maximum for $\beta=0.075$. We believe that this discrepancy is at least partly due to our not being able to take multiple scattering into account properly. The reason for this can be understood by examining the first moment ratio R as a function of κ in Fig. 9. At $\kappa = 2.2 \text{ \AA}^{-1}$ we have overestimated the multiple-scattering correction which leads to a deeper minimum in the experimental L . Similarly, for lower values of κ we have underestimated the multiple-scattering correc-

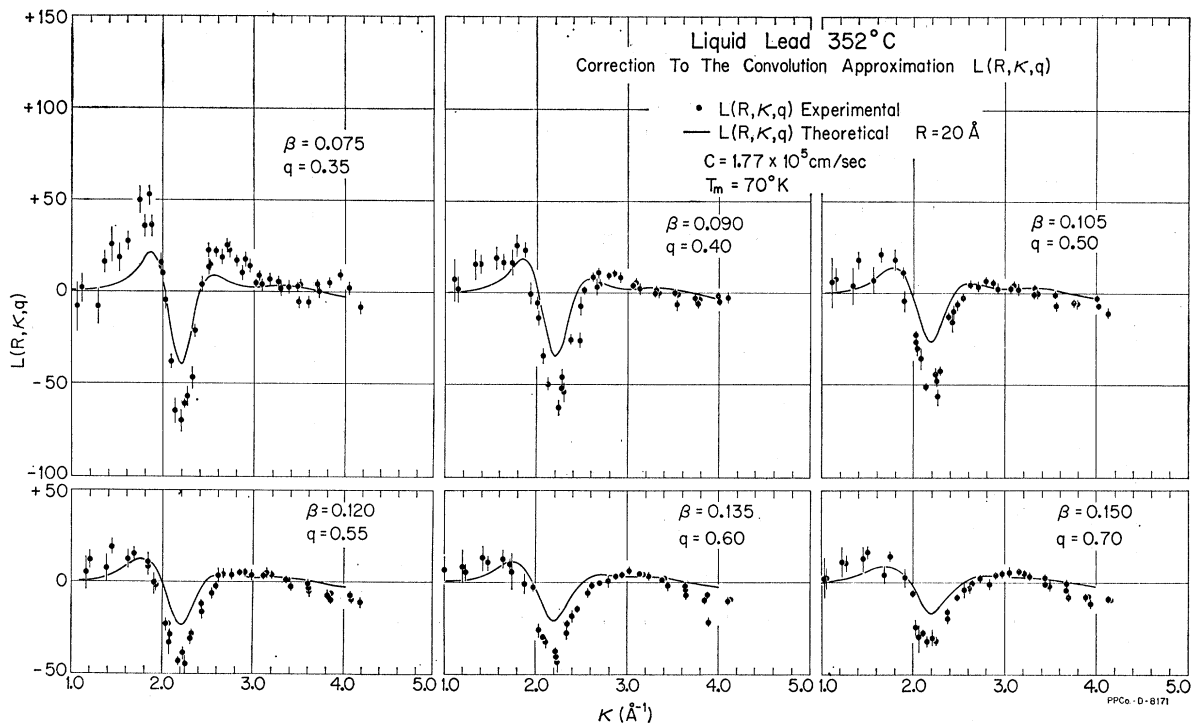


FIG. 12. Comparison of measured and theoretical values of $L(R, \kappa, q)$.

tion which leads to larger values of the left-hand maximum. How much of this discrepancy is due to multiple scattering alone we do not know. It could also partly be due to an inadequacy in the model.

It was mentioned earlier in this section that we had chosen a linear dispersion law with the velocity of sound $C = 1.77 \times 10^5$ cm/sec. The q values shown in Fig. 12 for the various values of β correspond to this velocity of sound and seem to give an L function which fits reasonably well with observation. For example, a value of $q = 0.70 \text{ \AA}^{-1}$ for $\beta = 0.09$ would not give as good an agreement. This would imply a value of $C = (4/7) \times 1.77 \times 10^5$ cm/sec. Nor would a value of q much less than 0.4 \AA^{-1} give a reasonable fit. From our observations all we can say about C is that a value of 1.8×10^5 cm/sec is a reasonable one, and we cannot make any statement about a deviation from a linear dispersion law.

It is important to realize that although T_m occurs as a parameter in the model and the form of $f(\omega)$ has been chosen somewhat arbitrarily, the κ structure of the experimental L function from which we have tried to deduce the collective aspects of the motion in a liquid is independent of the above choice. As is obvious from the theoretical expression for $L(R, \kappa, q)$ [Eq. (12)], this structure depends only on $\Gamma(\kappa)$ and q . With an increase in sample temperature one would expect the structure to broaden.

We have calculated the one-phonon scattering law for various values of T_m ranging from 50 to 80°K and found

that $T_m = 70^\circ\text{K}$ gives the most satisfactory agreement. The calculation is rather insensitive to the value of the coherence radius R for $R \geq 15 \text{ \AA}$, and we have from previous experience chosen $R = 20 \text{ \AA}$. We have also obtained an experimental $L(R, \kappa, q)$ using Sharrah's¹⁵ neutron values of $1 + \Gamma(\kappa)$ and found not quite as good an agreement. The width of the minimum in the experimental $L(R, \kappa, q)$ in this case is somewhat broader in comparison with the model than the width obtained with x-ray values of $1 + \Gamma(\kappa)$.

To get an approximate idea of the "quasi-phonon" dispersion curve without any reference to a model and drawing from analogy with a polycrystalline solid, we have obtained the dynamical structure factor $Z_{\text{liq}}[\mathbf{k}, \omega(q)]$ by dividing the observed $S_{R, \text{coh}}^{1\text{ph}}(\mathbf{k}, \hbar\omega)$ by calculated values of $S_{\text{inc}}^{1\text{ph}}(\mathbf{k}, \hbar\omega)$. This, when plotted as a function of κ at a constant β , exhibits two broad peaks, one on either side of $\kappa = 2.2 \text{ \AA}^{-1}$ for $\beta \gtrsim 0.90$. In Fig. 13 the positions of these peaks are plotted as a function of κ . The solid lines drawn through $\kappa = 2.2 \text{ \AA}^{-1}$ represent the linear dispersion law corresponding to $C = 1.77 \times 10^5$ cm/sec. Also shown are the points of Cocking and Egelstaff,⁴ as well as those of Dorner *et al.*²⁸ The shaded region shows the longitudinal dispersion curves obtained by Brockhouse *et al.*²⁹ from single-crystal measurements for the three symmetry

²⁸ B. Dorner, T. Plesser, and H. Stiller, *Physica* **31**, 1537 (1965).

²⁹ B. N. Brockhouse, T. Arase, G. Caglioti, K. R. Rao, and A. D. B. Woods, *Phys. Rev.* **128**, 1099 (1962).

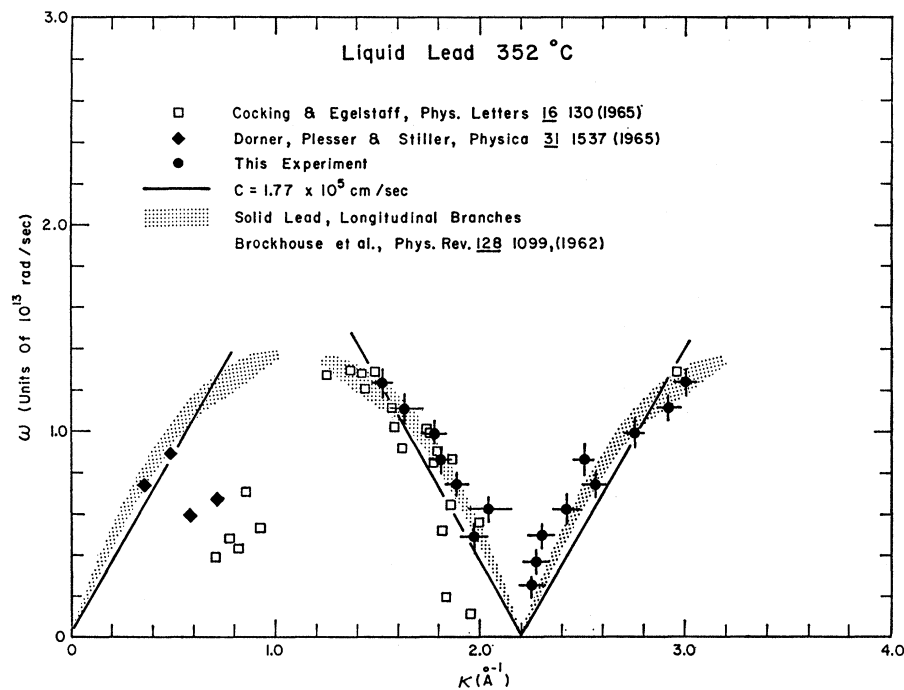


FIG. 13. The dispersion curve for liquid lead obtained from this experiment compared with other measurements.

directions [100], [110], [111]. The vertical error bars are due to energy resolution and horizontal bars are due to our estimated uncertainty in establishing the position of the peaks. An interesting feature of this plot is that by virtue of the fact that the dispersion curve is obtained on both sides of $\kappa = 2.2 \text{ \AA}^{-1}$ one is led to believe in the existence (for times $\sim 10^{-12}$ sec) of a second "Brillouin zone" in the liquid. The center of this second zone, which presumably is located at $\kappa \leq 2.2 \text{ \AA}^{-1}$, is, however, rather fuzzily defined because of the finite width of the diffraction maximum.

VII. CONCLUSIONS

There is not only a qualitative but also a semi-quantitative agreement between the predictions of the QC model and our observations. In this connection it is important to realize that our conclusions regarding the collective aspects of the motion, which have been derived from the dynamical structure factor $Z_{\text{liq}}(\kappa, \omega)$ or more precisely from the term containing the L function, do not depend on the parameters of the model. When better experimental data are available and multiple scattering corrections can be handled with

reliability, it would be interesting to refine the model by taking into account the longitudinal and the transverse character of the collective modes. It might then also be possible to estimate the range of the coherence parameter R .

If one tries to understand the experimental results on a phenomenological basis as we have done in this paper, one arrives at the conclusion that there do exist high-frequency "collective excitations" in a classical liquid which obey a certain average dispersion law which, in contrast to that in a solid, is more like a ribbon in the ω - q plane. Also, there exist Brillouin zones, at least the first two, in liquid lead. These zones are no doubt diffuse. It is, therefore, not very surprising that the scattering law $S(\kappa, \omega)$ in a liquid beyond the "quasi-elastic" region is very similar to that of a polycrystalline solid.

ACKNOWLEDGMENTS

We are indebted to Dr. R. M. Brugger for advice and many stimulating discussions. One of us (P.D.R.) wishes to thank Argonne National Laboratory for its hospitality and Phillips Petroleum Company for supporting his stay there.